INTERNATIONAL JOURNAL OF AUTOMOTIVE AND MECHANICAL ENGINEERING
ISSN: 2229-8649 e-ISSN: 2180-1606
VOLUME 23, ISSUE 3, 2026, 13773 - 13787
DOI: https://doi.org/10.15282/ijame.23.3.2026.3.1039

RESEARCH ARTICLE

Numerical analysis of energy harvesting characteristics in axially functionally graded beam structures with different geometric profiles for automotive application

Rasmi Ranjan Senapati[1], Alok Ranjan Biswal[2], Abinas Bibek Dash[1], Satyakam Acharya[1], Deepak Ranjan Biswal[2]*

[1]Department of Mechanical Engineering, DRIEMS University, Cuttack, Odisha, 754022, India
[2]Faculty of Department of Mechanical Engineering, DRIEMS University, Cuttack, Odisha, 754022, India

Abstract - This study presents a wide-ranging numerical investigation of the energy-harvesting characteristics of an axially functionally graded beam structure with different geometric profiles. Axially functionally graded materials (FGMs) offer exceptional advantages in energy harvesting applications because their varying material properties in the length direction can be optimised for energy conversion. In this study, the finite element method (FEM) was used to compare different beam configurations and analyse them under dynamic loading conditions. Three different geometric profiles, namely uniform, linear, and parabolic variations along the length direction, were used in this analysis. Each profile consists of a piezoelectric layer near the fixed end of the functionally graded beam, enabling it to serve as an energy-harvesting system. The material properties of the beam follow a distribution function that defines the grading profiles. To determine key performance parameters, such as power generation, voltage output, and natural frequencies under various excitation conditions, MATLAB was used. Both geometric taper ratios, namely, the width taper and height taper, were used for the analysis, and their influence on the overall performance was studied. The results obtained through numerical analysis provide valuable insights for the proper design of an energy-harvesting device that can be used in autonomous micro-electromechanical systems, structural health monitoring, and wireless sensor networks. The parabolic-profile beam exhibited an approximately 115% higher voltage response than the uniform beam, indicating a significantly enhanced electromechanical performance.

Article History
Received : 27 July 2025
Revised : 12 February 2026
Accepted : 11 March 2026
Published : 25 September 2026

Keywords
Energy harvesting
Geometric profiles
Axially functionally graded beam
Modal analysis

1. Introduction

The rapid demand for self-sustaining and autonomous electronic systems has significantly increased research in the field of energy harvesting technologies, which capture energy from the surrounding environment [1]. Among several existing mechanisms, vibration-based energy harvesting has been recognized as a promising solution for powering low-power electronic devices, particularly in applications where replacing batteries is impractical or costly [2]. This ability to convert mechanical energy into electric power offers a viable solution for micro-electromechanical systems, such as structural health monitoring, wireless sensor networks, and Internet of Things (IoT) devices [3]. Functionally graded materials (FGMs) play a significant role in this context and are composite materials with varying material properties [4]. Unlike traditional composites, FGMs exhibit smooth transitions in mechanical, thermal, and electrical properties, thereby reducing stress concentrations and interface delamination. Because of their unique properties, FGMs play a key role in various engineering fields, including aerospace, biomedical, and energy conversion systems [5]. Furthermore, combining FGM with piezoelectric materials unveils new possibilities for improving the energy conversion efficiency [6]. In this context, axially functionally graded beams offer greater tunability of dynamic characteristics to satisfy specific operational requirements. Variations in material properties help to optimise the frequency response and power output [7]. The design of energy-harvesting beams is a critical factor that affects their dynamic behaviour and energy conversion performance. To achieve this, different configurations, such as uniform, tapered, exponential, and polynomial profiles, and their performance, such as modal behaviors and stress distributions under dynamic loads, were examined. Advances in computational mechanics and finite element techniques now allow for a more precise study of complex interactions in FGMs. The finite element method provides researchers with a powerful tool for investigating the interactions among mechanical vibrations, material properties, and electromechanical coupling in piezoelectric energy-harvesting systems [8]. Computer simulations enable parametric studies that would be too expensive or time-consuming to conduct with physical experiments. Researchers have studied nonuniform functionally graded piezoelectric cantilever beams under harmonic excitation using Euler, Bernoulli, and Timoshenko beam theories, as well as finite element methods. They compared the simulation results with existing experimental results. However, this method has limitations because it relies solely on simulations and does not involve new experiments. It uses idealized conditions that may not fully represent real-world situations [9].

Recent studies have focused on harvesting energy from axially functionally graded piezolaminated nonprismatic beams for automotive applications under both mechanical and thermal loading conditions. Researchers have developed a multiphysics finite-element model to simulate tapered cantilever beams with varying height-to-width taper ratios while keeping the material gradient parameters constant. The results show that adding thermal loading significantly increased both the displacement and power output amplitudes. Optimized taper designs reached up to 0.15 W/mm², a 650%

*CORRESPONDING AUTHOR| D. R. Biswal | ✉ deepakrbiswal@gmail.com
© 2026 The Authors. Published by Universiti Malaysia Pahang Al-Sultan Abdullah Press. This is an open access article under the CC BY-NC 4.0 license

improvement over the mechanical loading alone. Voltage generation also decreased with greater tapering in both the height and width directions. One major limitation is that the material gradient parameters (k = 1, np = 4) remained fixed, which could make it harder to apply these results to other materials and shapes in real-world use [10]. The modified couple-stress theory was used to examine rotating micro-disks with functionally graded materials in two directions, subjected to both heat and pressure. The Material properties change with temperature and vary along the thickness and radius. Hamilton's principle and the Ritz method have been used to solve the equations in analyses that include geometric nonlinearity. The model accounts for thermal, centrifugal, and pressure effects, and the corresponding influences of parameters such as temperature, speed, pressure, and material gradation on the disks [11]. A new approach for vibration energy harvesting was examined, where a bimorph pipe with functionally graded materials in three directions carried a steady fluid flow. The material properties change along the width, height, and length directions, and electricity is generated by the piezoelectric layers on the surfaces. Finite element simulations of voltage and power verified the theoretical results. This study assessed the effects of material gradients, fluid-structure interactions, load resistance, and geometry on performance. The results show that the maximum output power can be achieved at a lower resistance owing to changes in the axial and height gradients. Nevertheless, the system becomes unstable at higher fluid speeds, which may cause energy harvesting to fail and confine its use in fast-flowing applications [12].

Further studies examined axially functionally graded piezoelectric beam materials and their effect on vibration behavior due to property variation along the beam length in exponential and power-law distributions. In that study, the effects of natural frequencies owing to changes in the volume fraction, slenderness ratio, and different boundary conditions were studied. Specific boundary conditions, such as fixed-free and fixed-fixed, have been considered without accounting for temperature and damping effects, which may limit their applicability to more complex real-world structures [13]. To improve the performance of functionally graded piezoelectric energy harvesters with geometric nonuniformity, some researchers have used the Lichtenberg Algorithm and Artificial Neural Networks. In that study, greater emphasis was placed on the thickness of the piezoelectric layers and tapering ratio to achieve maximum voltage. Finite element-based analysis within Kirchhoff plate theory has been used to model electromechanical behavior using four-node elements. The Lichtenberg Algorithm was used to solve problems more efficiently, whereas neural networks were used to train the simulation data to obtain optimal design parameters. However, this approach relies on idealized models and pre-made training datasets and may not readily generalize to a wide range of real-world situations [14]. Further research has examined the vibration frequencies of functionally graded beams with axial non-homogeneity in material properties and point masses. In that study, the authors used a precise integration approach and scaled boundary finite element method. This method employs high-order elements only along the beam length, sets up a first-order matrix equation and a dual vector method, and solves it using a precise integration approach to obtain accurate stiffness and mass matrices. Although this method predicts natural frequencies well and examines the effects of material gradients, boundary conditions, and mass distribution, it assumes linear elasticity, neglects damping, and employs idealized boundary conditions [15].

Researchers have studied functionally graded plate structures supported by elastic foundations with varying stiffnesses under different boundary conditions. A quasi-three-dimensional model combines the nonlocal strain-gradient theory with cosine-based material gradation. We used a hybrid hyperbolic-parabolic approach to address the shear deformation. We implemented the Virtual Work method to derive the governing equation, which we solved using the Galerkin approach. In this process, both larger plates and nanoplates were used, and the results were compared with those previously reported. The behavior was studied in detail under the influence of the foundation properties, size, and boundary conditions. However, this analysis did not consider the dynamic and thermal effects [16]. In continuation of this, a higher-order shear deformation theory has been used for analyzing functionally graded porous (FGP) beams and buckling and free vibration in laminated composite (LC) beams. In this study, the governing equation was derived using Lagrange's principle, and the resulting equations were solved using Legendre-Ritz functions, accounting for porosity variations and various edge constraints. However, this approach neglects the dynamic and thermal effects. Consequently, it is limited to a narrow range of engineering applications [17]. The stability of functionally graded elliptical pipes carrying fluid was analyzed, considering nonuniform flow velocity profiles. This approach employs Timoshenko beam theory, which accounts for the Coriolis and Centrifugal forces in elliptical geometries. The finite element method with modal analysis was employed. In this study, linear material properties and ideal fluid behavior were used. The corresponding effects were studied on elliptical cross-sections. Consequently, it was limited to other geometries and real-world scenarios [18].

An energy harvester made of Garolite FR-4 epoxy laminate with variable thickness was studied. In the theoretical analysis, Euler-Bernoulli beam theory was used, and the Rayleigh-Ritz method was used to solve the equation. A variable-thickness model shows a more uniform strain distribution, increasing efficiency above 75% [19]. Both Euler–Bernoulli and Timoshenko beam theories were used for the numerical solution and experimental validation of non-graded beams under bridge vibrations caused by moving vehicles. A previous study used an ideal material gradation and simplified structural model [20]. Recently, the vibration characteristics of an axially functionally graded non-prismatic beam were investigated using Timoshenko beam theory under axial thermal variations in a humid environment. The beam had a varying thickness along the length direction and a constant width. The material properties were temperature-dependent and axially distributed according to a power law. The governing equation was derived using Hamilton's principle, and the harmonic differential quadrature method was used to solve it. The analysis used three thermal conditions: linear, nonlinear, and uniform temperature variation with a constant moisture concentration [21]. Recent advances in vibration energy harvesting and piezoelectric systems have focused on improving the energy conversion efficiency through innovative structural designs, analytical modeling, and experimental validation. Researchers developed a fully coupled

model of a quarter-wavelength resonator integrated with a piezoelectric backplate and experimentally validated its effectiveness for vibroacoustic energy harvesting [22]. Synergistic structural design approaches have significantly improved the performance of piezoelectric energy harvesters, enhancing their power generation capabilities [23]. Similarly, researchers have developed a closed-form analytical solution for energy harvesting in sandwich beams subjected to impact loading, providing valuable insights into the dynamic response and harvested energy characteristics of such systems [24]. In vibration-based diagnostics, researchers have investigated the effect of sensor placement on engine misfire detection using artificial neural networks and have shown that appropriate positioning significantly improves detection accuracy [25]. These studies collectively highlight the growing importance of advanced modeling techniques, structural optimization, and intelligent sensing methodologies for enhancing the performance of energy harvesting and vibration monitoring systems. To establish the practical relevance of the proposed energy-harvesting system, particularly for automotive applications, a detailed analysis of realistic vehicle vibration is required. Automotive vibrations arise primarily for two reasons: first, they arise from road conditions, which vary from poor to good. Second, engine vibrations induce them. We evaluated the performance of the proposed profile beam under these realistic excitation scenarios to identify the power-generation potential, frequency strategies, and optimal design parameters. This is important for real-world automotive use. Table 1 presents a detailed comparison between the existing approach and the methodology used in this study.

Table 1. Comparison of existing approaches with the present study

Existing Approaches	Present Study	New Knowledge Contribution
Primarily transversely graded FGMs; uniform material distribution along the beam length [26]	Axially functionally graded structures with spatially varying properties	Systematic analysis of axial gradation effects on energy harvesting performance under automotive vibrations
Predominantly uniform rectangular cross-sections; limited geometric variation [27]	Multiple profiles: uniform, linear and parabolic configurations	Comprehensive mapping of geometry-gradation synergy for optimised power density
Idealised harmonic or base excitation; single frequency analysis [28]	Realistic automotive vibration spectra from multiple vehicle zones	Application-specific design guidelines for different vehicle mounting locations
Focus on a single objective (power output or bandwidth) [29]	Multi-objective optimisation: power density, bandwidth, and structural durability	Integrated performance metrics for practical automotive implementation
Separate analysis of material or geometric effects [30]	Coupled finite element analysis integrating both gradation and geometry	Predictive model correlating Axially Functionally graded patterns with geometric profiles for enhanced harvesting efficiency
General vibration energy harvesting; laboratory conditions [31]	Automotive-specific: suspension, engine mount, exhaust system vibrations	Vehicle-ready design specifications and optimal configuration recommendations

As the automotive industry rapidly electrifies, there is a growing need for new energy recovery systems to improve vehicle efficiency and reduce reliance on conventional batteries. One major method is to harvest piezoelectric vibration energy using functionally graded materials that offer better electrical and mechanical properties. Axially functionally graded beam structures, in which the material properties vary along the beam length, can convert energy more effectively than uniform beams. Although several studies have examined transversely graded piezoelectric energy harvesting, the combined effect of changes in beam shape and axial grading has not been investigated in automotive settings. Few numerical frameworks relate different beam shapes, such as linear, parabolic, and uniform, to axial gradient patterns. This study addresses these gaps and examines the effects of beam geometry and material grading on the output power.

2. Materials and Methods

The mathematical formulation models an axially functionally graded beam with different geometries, material nonhomogeneity along its length, and an electrical interface for measuring the power output. The beam is axially functionally graded, and its material properties change along its length. The mathematical expressions for these functionally graded features with uniform, linear, and parabolic distribution profiles are expressed as follows:

$$E(x) = E_0 \left[1 + k_e \left(\frac{x}{L}\right)\right] \tag{1}$$

$$\rho(x) = \rho_0 \left[1 + k_{p1} \left(\frac{x}{L}\right) + k_{p2} \left(\frac{x}{L}\right)^2\right] \tag{2}$$

where $E(x)$ and $\rho(x)$ are the Young's modulus and density of the beam material, respectively. The terms k_e, k_{p1}, and k_{p2} are dimensionless coefficients that determine the shape of the gradients and are equal to unity. Young's modulus varies linearly, whereas the density varies parabolically along the beam length. Eq. (3) presents the equations for the cross-

sectional area of a uniform-profile beam. Similarly, Eqs. (4-5) present the formulations for the cross-sectional areas of the linear and parabolic profile beams.

$$A(x) = A_0 \tag{3}$$

$$A(x) = A_0\left[\left(1-\alpha\frac{x}{L}\right)\left(1-\beta\frac{x}{L}\right)\right] \tag{4}$$

$$A(x) = A_0\left[\left(1-\alpha\frac{x}{L}\right)^2\left(1-\beta\frac{x}{L}\right)^2\right] \tag{5}$$

The length of the beam is *L*, and the transverse cross-sectional area is A0, near the clamped end. *where α and β re*present the width and height tapers for the linear and parabolic profiles, respectively, and range from 0 to 1. The cross-sectional area of the beam was modeled using three different geometric profiles: uniform, linear, and parabolic, as shown in Figure 1.

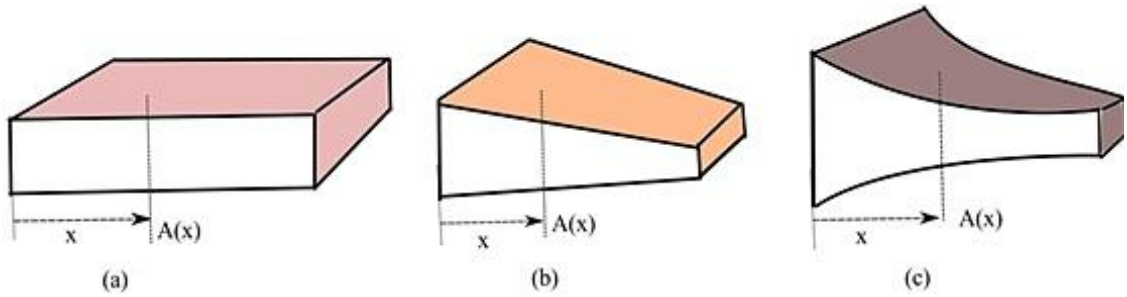


Figure 1. Geometric profiles of the piezo-electric energy harvester: (a) uniform beam, (b) linearly tapered beam, and (c) parabolically tapered beam

The beam displacement components along the three mutually perpendicular directions *x, y,* and *z* can be expressed as Eq. (6).

$$\begin{aligned} u(x,y,z,t) &= -k\theta(x,t) = -k\left(\frac{\partial w}{\partial x}\right) \\ v(x,y,z,t) &= 0 \\ w(x,y,z,t) &= w(x,t) \end{aligned} \tag{6}$$

The beam element was subjected to two degrees of freedom at each node. In finite element modeling, each nodal point is assumed to experience two degrees of freedom, namely transverse displacement (*v*) and rotation (*ψ*), which are developed due to the shear force and bending moment. The three-dimensional constitutive equations of piezoelasticity can be represented as in Eqs. (7-8).

$$\{\sigma\} = [\bar{C}]^E\{\varepsilon\} - [\bar{e}]\{E_e\} \tag{7}$$

$$\{D\} = [\bar{e}]^T\{\varepsilon\} + \left[\bar{\xi}\right]^S\{E_e\} \tag{8}$$

where *σ*, *ε* are stress and strain tensors, $\bar{C}$ are the compliance matrix coefficients; E_e represents a vector of applied electric field, respectively. Parameter *D* represents the electric displacement vector. The terms $\bar{e}$ denotes the piezoelectric coupling coefficient, ξ represents the permittivity, and $\mathcal{E}$ represents the pyroelectric tensor. Furthermore, because the structure is modeled using Euler–Bernoulli beam theory, all stress components except the one-dimensional bending stress (σ_1) are considered negligible, modifying the equations expressed in Eqs. (9-10).

$$\sigma_1 = \bar{c}_{11}^E\varepsilon_1 - \bar{e}_{31}E_3 \tag{9}$$

$$D_3 = \bar{e}_{31}\varepsilon_1 + \bar{\xi}_{33}^S E_3 \tag{10}$$

In the present method, for the piezo-electric layer, a single electrical degree of freedom is assumed. The electric potential difference between the top and bottom surfaces of the piezo-electric material is kept constant, while its variation across the transverse direction is linear and is expressed in Eq. 11.

$$-E_{33} = [B_v]\{v\} \tag{11}$$

where B_v is the electric field gradient matrix of the piezo-electric patch, and *v* is the applied voltage. An axially Functionally Graded cantilever with three different profiles, such as uniform, linear and parabolic profiles, with a piezo-electric patch of length *Lp* near the clamped end, is shown in Figure 2.

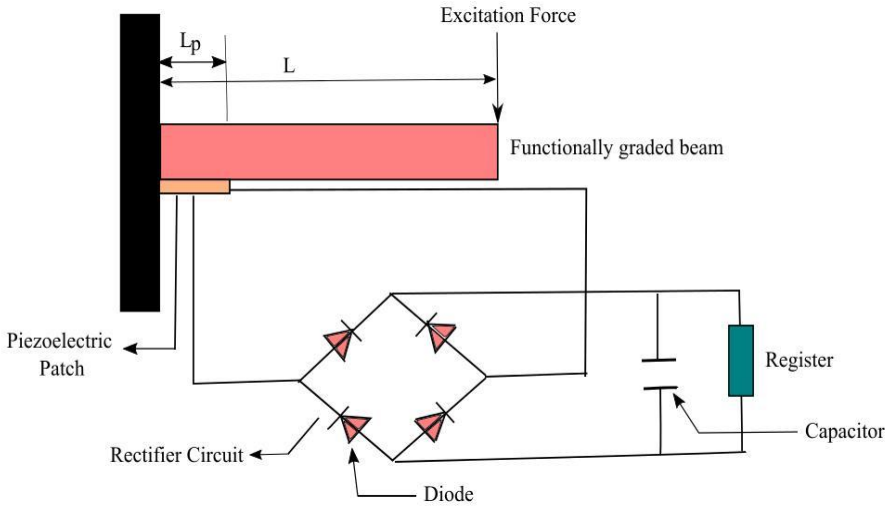


Figure 1. A piezo-laminated axially functionally graded beam having uniform/linear/parabolic profile cross sections with a classic electric interface for vibration energy harvesting

The free end of the proposed beam is subjected to a point load *F(t).* The dynamic equations of motion for an energy harvesting system can be described using Hamilton's principle as

$$\Pi = \int_{t_1}^{t_2} [\partial(E_k - E_p + W_e) + \delta W]dt = 0 \tag{12}$$

E_k is the kinetic energy, E_p is the total electromechanical enthalpy, W_e *is* the work done by the electrical force, and δW is the work done owing to the external mechanical and electrical loads. t_1 and t_2 are the time constants at which the first variations vanish. This equation can be used to analyse any mechanical system comprising piezoelectric patches. The equation of motion of the piezo-laminated, discretized structure is illustrated by

$$\begin{bmatrix} M_b + M_p & 0 \\ 0 & 0 \end{bmatrix} \begin{Bmatrix} \ddot{q} \\ \ddot{v} \end{Bmatrix} + \begin{bmatrix} C & 0 \\ 0 & 0 \end{bmatrix} \begin{Bmatrix} \dot{q} \\ \dot{v} \end{Bmatrix} + \begin{bmatrix} K_b + K_p & K_{bp} \\ K_{pb} & -K_{pp} \end{bmatrix} \begin{Bmatrix} q \\ v \end{Bmatrix} = \begin{Bmatrix} Q \\ 0 \end{Bmatrix} \tag{13}$$

In addition, the system incorporates supplementary structural damping, which must be considered in the analysis. The structural damping was modelled using proportional damping. The stiffness and mass matrices are computed by numerical integration using the 2-point Gauss quadrature method. The dynamic behavior of the piezo-thermoelastic beam was determined using the Newmark method. This approach transforms the governing differential equations of motion into a set of algebraic equations, as follows.

$$\left[K_{eff}\right]^{t+\Delta t}\{q\} = Q_{eff} \tag{14}$$

where K_{eff} and Q_{eff} are the effective stiffness matrix and effective load vector, which can be found as

$$K_{eff} = \left([K_b] + [K_p] + [K_{pb}][K_{pp}]^{-1}[K_{bp}]\right) + a_0([M_b] + [M_p]) + a_1[C] \tag{15}$$

$$Q_{eff} = \left[M_b + M_p\right]\{a_0(q_t) + a_2(q_t) + a_3(q_t)\} + [C]\{a_1(q_t) + a_4(q_t) + a_5(q_t)\} \tag{16}$$

The terms $a_0, a_1, a_2, a_3, a_4, a_5$ are represented as

$$a_0 = \frac{1}{\varepsilon \Delta t^2}\ ;\ a_1 = \frac{\delta}{\epsilon \Delta t}\ ;\ a_2 = \frac{1}{\epsilon \Delta t}\ ;\ a_3 = \frac{1}{2\varepsilon} - 1\ ;$$
$$a_4 = \frac{\delta}{\epsilon} - 1\ ; a_5 = \frac{\Delta t}{2}\left(\frac{\delta}{\epsilon} - 2\right)\ ; \epsilon = 0.25; \delta = 0.5. \tag{17}$$

To calculate the output power of the piezoelectric beam, it is presumed that the deformation profile of the beam remains unchanged, even though there is a slight increase in the bending stiffness due to the piezoelectric layer. The resulting output voltage from the deformation of the PZT patch can be expressed as

$$[K_{pp}]^{-1}[K_{p\theta}]\{\theta\} + [K_{pp}]^{-1}[K_{pb}]\{q\} \tag{18}$$

For a purely resistive load, the relation between voltage and power can be represented as

$$P_{output} = \frac{v^2}{R_l} \tag{19}$$

3. Results and Discussion

The Finite element formulation was used to obtain results for the three geometric profiles of axially functionally graded beams. This section discusses the power-generation capabilities of these profiles and compares the voltage outputs, natural frequencies, and energy conversion efficiencies. The influence of geometric parameters and material gradient indices on the overall harvesting performance has also been studied. For this purpose, the first three nondimensional natural frequencies of the uniform beam were initially calculated as a benchmark using the following equation:

$$\omega_{non-dimensional} = \omega \times L^2 \times \sqrt{\frac{\rho A}{EI}} \tag{20}$$

Table 2 presents a comparative sensitivity analysis of the beam using the Euler-Bernoulli and Timoshenko beam theories. The comparison is based on the non-dimensional frequencies for the first three modes of vibration. The deviation between the two theories is negligible.

Table 2. First three nondimensional frequencies of the beam using Euler-Bernoulli and Timoshenko beam theories

Parameter	Mode	Euler–Bernoulli Beam theory	Timoshenko Beam theory	Deviation (%)
Nondimensional Frequency	1	3.5160	3.5155	0.0142
Nondimensional Frequency	2	22.0345	22.0312	0.0149
Nondimensional Frequency	3	61.6982	61.6889	0.0150

Similarly, Table 3 presents the first three dimensionless natural frequencies of a uniform beam with one end fixed and the other end free in the energy-harvesting analysis. The fundamental non-dimensional frequency was 3.082, corresponding to the primary vibrational mode that is most relevant for energy conversion applications. The second and third modes appear at 19.312 and 54.083, respectively, showing the characteristic frequency progression of beam structures. These nondimensional values provide a vital baseline for comparative analyses with other geometric profiles, such as linear and parabolic configurations. The fundamental mode offers the maximum energy-harvesting potential owing to its optimal displacement amplitude, whereas higher modes contribute to a broadband frequency response.

Table 3. First three nondimensional natural frequencies of a uniform beam with a piezo patch near the fixed end

1st Nondimensional natural frequency	3.082
2nd Nondimensional natural frequency	19.312
3rd Nondimensional natural frequency	54.083

Table 4. First nondimensional Natural frequency of a linear and parabolic profile beam with variation in width taper (α) = 0.0, 0.3, 0.5, 0.7 and variation in height taper (β) = 0.0, 0.3, 0.5, 0.7

Value of β	α = 0		α = 0.3		α = 0.5		α = 0.7	
	Linear	Parabolic	Linear	Parabolic	Linear	Parabolic	Linear	Parabolic
β = 0	3.082	3.082	3.164	3.216	3.213	3.228	3.236	3.072
β = 0.3	2.690	2.105	2.706	2.030	2.697	1.905	2.649	1.674
β = 0.5	2.306	1.313	2.278	1.203	2.235	1.086	2.649	1.674
β = 0.7	1.783	0.624	1.725	0.550	1.663	0.482	1.567	0.395

Table 4 illustrates the first nondimensional natural frequencies for beams with linear and parabolic taper profiles, considering variations in both the width taper (α) and height taper (β). To assess the influence of geometric tapering on the dynamic behaviour of the beam, the taper values were varied between 0.0 and 0.7. It was observed that increasing the width taper (α) while keeping the height of the beam (β = 0) constant resulted in a slight increase in the natural frequency, which was more noticeable for the linear profile. However, a significant reduction in frequency was observed for both profiles, particularly in the parabolic case, as the height taper increased. This is due to the significant decrease in beam stiffness, which reduces the natural frequencies. Furthermore, parabolic profiles consistently exhibit lower frequencies than linear profiles under the same variation in tapers owing to the curved geometry. The most considerable frequency drop of nearly 0.395 rad/s occurs at the highest taper values (α = 0.7 and β = 0.7) in the parabolic beam.

Similarly, Table 4 presents the second nondimensional natural frequencies of the beam with parabolic and linear taper profiles. The width taper (α) and height taper (β) varied between 0.0 and 0.7. By increasing the width taper (α) and keeping the height taper intact (β = 0), the natural frequencies with parabolic profiles generally show higher or comparable values than linear ones. However, as the height taper (β) increases, the nondimensional natural frequencies consistently decrease for both beam profiles, with a more significant decrease in the parabolic case. For the same taper values, the parabolic profile exhibited sharper frequency reductions than its linear counterpart. Furthermore, for taper levels (α = 0.7 and β = 0.7), the nondimensional natural frequency dropped to 2.483 for the parabolic profile and 9.828 for the linear profile. This is due to the greater reduction in structural stiffness, which results in greater flexibility in the dynamic behaviour. It was

concluded that the height taper has a significant effect on the second mode of vibration frequency compared to the width taper, and the parabolic profile geometry shows a greater reduction in amplification.

Table 1. Second nondimensional Natural frequency of a linear and parabolic profile beam with variation in width taper (α) = 0.0, 0.3, 0.5, 0.7 and variation in height taper (β) = 0.0, 0.3, 0.5, 0.7

Value of β	α = 0	α = 0.3	α = 0.5	α = 0.7

Table 5. Second nondimensional Natural frequency of a linear and parabolic profile beam with variation in width taper (α) = 0.0, 0.3, 0.5, 0.7 and variation in height taper (β) = 0.0, 0.3, 0.5, 0.7

Value of β	α = 0		α = 0.3		α = 0.5		α = 0.7	
	Linear	Parabolic	Linear	Parabolic	Linear	Parabolic	Linear	Parabolic
β = 0	19.312	19.312	19.825	20.151	20.130	20.225	20.278	19.259
β = 0.3	16.853	13.189	16.953	12.727	16.897	11.947	16.600	10.507
β = 0.5	14.445	8.227	14.274	7.544	14.007	6.814	16.600	10.507
β = 0.7	11.176	3.908	10.818	3.448	10.432	3.028	9.828	2.483

Table 6. Third nondimensional Natural frequency of a linear and parabolic profile beam with variation in width taper (α) = 0.0, 0.3, 0.5, 0.7 and variation in height taper (β) = 0.0, 0.3, 0.5, 0.7

Value of β	α = 0		α = 0.3		α = 0.5		α = 0.7	
	Linear	Parabolic	Linear	Parabolic	Linear	Parabolic	Linear	Parabolic
β = 0	54.083	54.083	55.508	56.417	56.356	56.626	56.771	53.953
β = 0.3	47.177	36.918	47.458	35.642	47.306	33.479	46.486	29.473
β = 0.5	40.438	23.039	39.966	21.145	39.226	19.114	46.486	29.473
β = 0.7	31.298	10.948	30.306	9.670	29.234	8.499	27.555	6.976

Table 6 summarises the third nondimensional natural frequency of the beams with linear and parabolic taper profiles. Both α and β vary in the range 0.0–0.7, showing a detailed combined geometric effect on the higher-mode vibration. It can be observed that the third dimensionless natural frequency increases gradually as the width taper α increases in the absence of the height taper (β = 0). However, when β increases, the nondimensional natural frequency decreases for both profiles, and this is more pronounced in the case of parabolic profiles. When both taper values (α = 0.7 and β = 0.7) are considered, the nondimensional natural frequency for the parabolic profile beam is 6.976, whereas that for the linear beam is 27.555. This reduction is due to the substantial loss of stiffness, particularly in a parabolic profile beam subjected to combined tapering. It was observed that the height taper has a greater effect on the third natural frequency than the width taper, and parabolic profile beams are more sensitive to such variations.

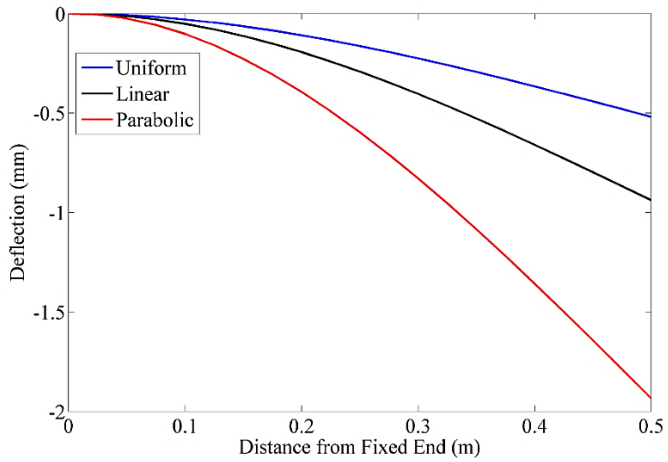


Figure 3. Deflection profiles of cantilever beams with uniform, linear, and parabolic cross-sectional geometries

Figure 3 represents the deflection profiles of three distinct cross-sectional geometries: uniform, linearly tapered, and parabolically tapered configurations. For this purpose, one end of the beam is fixed, and the other end remains free. The figure shows that geometric variation has a significant impact on structural response. It is observed that the tip displacement of the parabolic profile beam is approximately 2.0 mm, which is higher than that of the other profile beams. This is because a considerable reduction in cross-sectional area occurs toward the free end compared to other profiles. This results in a decrease in flexural rigidity and amplifies bending deformation, resulting in the maximum bending moment. In contrast, a uniform profile provides superior resistance to deflection due to constant stiffness along the length

of the beam. The linearly tapered profile produces an intermediate deflection of approximately 0.95 mm at the free end, representing a transitional case between the uniform and Parabolic profile beam.

Figure 4 illustrates the bending stress profiles at the top and bottom surfaces of the three cross-sectional geometries: uniform, linearly tapered, and parabolic. For this purpose, the end of the beam is subjected to a point loading, whereas the other end of the beam is fixed. From the figure, it is observed that the parabolic profile beam exhibits maximum tensile or compressive stress of approximately 10 MPa at the fixed support, indicating maximum material utilisation efficiency. Similarly, the uniform profile beam displays the maximum tensile or compressive stress of approximately 2.5 MPa, whereas in the linearly tapered configuration the value is approximately 5 MPa. From the figure, it is observed that the parabolic profile beam demonstrates superior stress distribution optimisation, resulting in a greater bending moment. Conversely, the uniform cross-section exhibits relatively low stress utilisation near the free end, suggesting material inefficiency. In order to validate the developed MATLAB code, a bimorph cantilever beam composed of two Polyvinylidene fluoride (PVDF) layers is analysed. The beam dimensions are specified as 100 mm in length, 5 mm in width, and 1 mm in thickness. It is discretised into five equal finite elements for numerical analysis. A unit voltage is applied across the thickness, and the resulting deflections are computed at five nodal points.

Table 7. Transverse deflection of a bimorph piezoelectric actuator

Distance(mm) from fixed end	Deflection (µm) [32]	Deflection (µm) [33]	Deflection (µm) present MATLAB code
20	0.0131	0.0138	0.0139
40	0.0545	0.0552	0.0554
60	0.1200	0.1240	0.1247
80	0.2180	0.2210	0.2218
100	0.3400	0.3450	0.3465

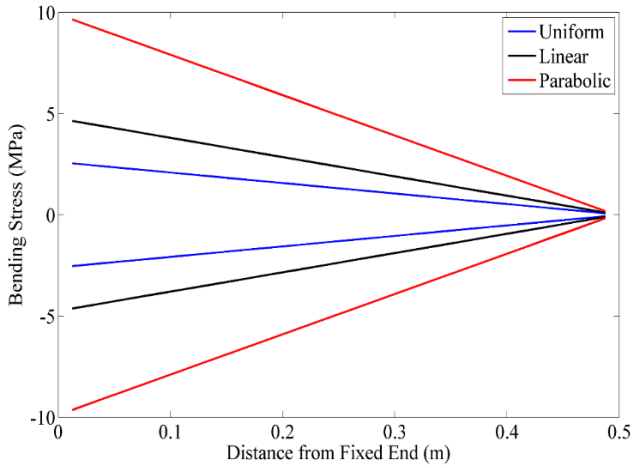


Figure 4. Bending stress distribution in cantilever beams featuring uniform, linearly tapered, and parabolic cross-sections

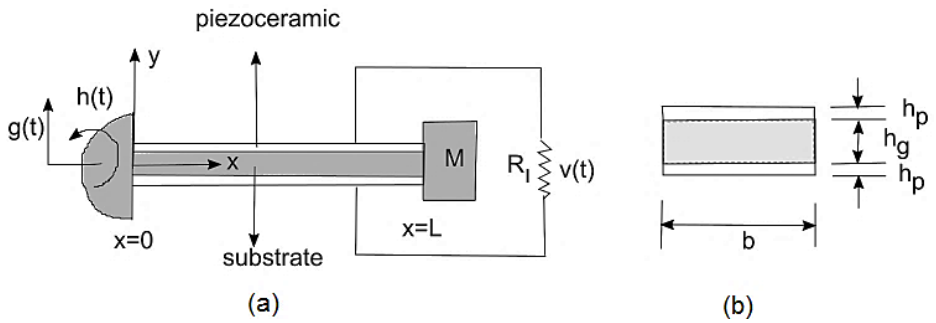


Figure 5. Bimorph cantilever configuration (a) with piezoceramic layers (b) cross-sectional view

Figure 6 (a-b) show the computed results of the voltage and current frequency response function (FRF) using the proposed formulation. Figure 6 (a-b) show that the present results are in close agreement with previously published experimental results [24]. A piezo-laminated cantilever beam under the simultaneous action of an impulse load at the free end and thermal load was analysed to study the output responses, such as displacement, voltage, and output power. The cross-sectional dimensions of the beam near the clamped end were taken as b_0 = 0.05 m and t_0= 0.004 m. The piezoelectric patch, with a length (Lp) of 0.05 m and thickness (tp) of 0.0005 mm, was attached near the clamped end of the beam with

a length of 0.5 m. The various mechanical, electrical and coupled material properties used near the clamped end are listed in **Error! Reference source not found.**.

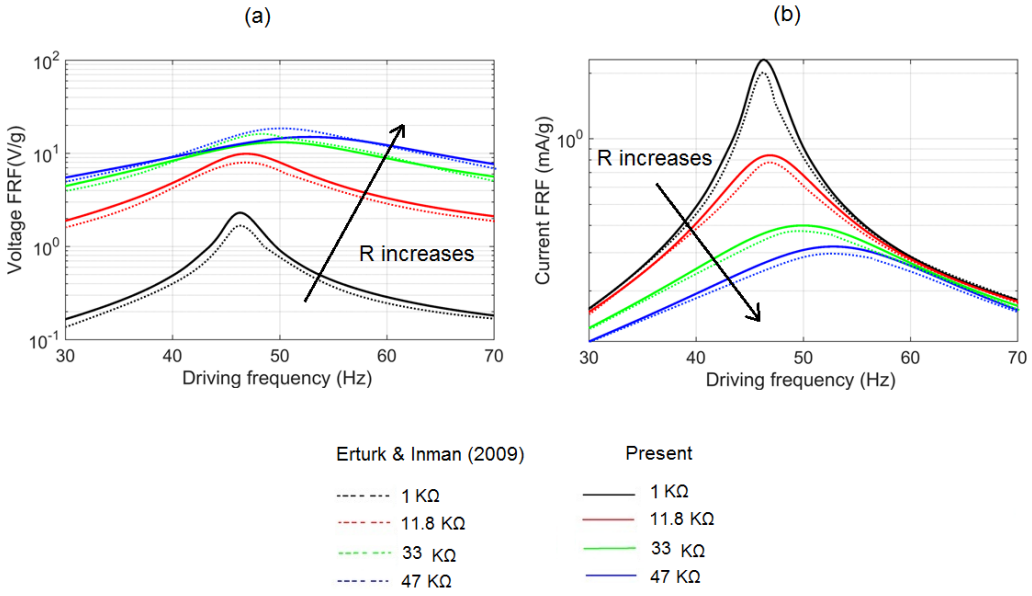


Figure 6. Comparison of voltage FRF for load resistances 1, 11.8 and 33 kΩ

Table 8. Material properties of the beam and PZT

Properties	Steel beam	PZT
E_0(Gpa)	210	0.0606
μ_0	0.3	*0.3*
G_0(Gpa)	80.7	0.0234
ρ_0(Kg m^{-3})	7850	7500
e_{31}(C m^{-2})	-	16.6
ε_{33}(nFm^{-1})	-	25.55

The following sections represent the frequency domain responses of the proposed beam profiles with variations in the width taper (α) and height taper (β). All results presented correspond to axially functionally graded beams incorporating spatially varying material properties, as defined in Eqs. (1-2). This represents an axial gradient index of unity for the linear variation in the modulus and quadratic variation in the density, consistent across all geometric configurations. Thus, the comparisons reflect the combined influence of the material gradation and geometric profile (uniform, linear, or parabolic) on the dynamic response and energy harvesting performance. Figure 7 shows the frequency-response characteristics of three types of profile beams: uniform, linearly tapered, and parabolically tapered beams. The system exhibited a frequency variation of up to 600 rad/s.

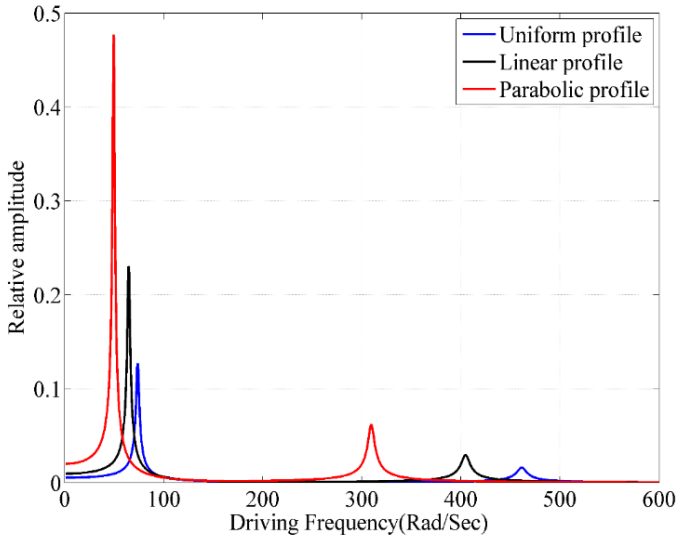


Figure 7. Frequency response of uniform profile beam (α = 0.0, β = 0.0), linear profile beam (α = 0.2, β = 0.3) and Parabolic profile beam (α = 0.2, β = 0.3)

For the preliminary parametric investigation, a width taper (α = 0.2) and height taper (β = 0.3) were selected. This is due to the avoidance of stress concentration, numerical instability, and excessive stiffness reduction. For lower taper values (i.e. α and β < 0.2), the harvested power and dynamic response remained close to those of uniform-profile beams, showing limited benefit from geometric modification. In contrast, higher taper values (i.e. α and β ≥ 0.5) lead to a pronounced reduction in the stiffness and natural frequencies of parabolic-profile beams. Intermediate values of α = 0.2 and β = 0.3 provide a compromise between stiffness and flexibility, resulting in an increase in the harvested power, output voltage, and vibration amplitude. It also clearly demonstrates the geometry–gradation synergy that interacts with the axial material gradation to concentrate the strain energy in the piezoelectric region near the fixed end. Therefore, α = 0.2 and β = 0.3 were selected as representative values to highlight the enhanced energy-harvesting performance and electromechanical coupling without affecting dynamic stability.

From Figure 7, it can be observed that the parabolic-profile system with α=0.2 and β=0.3 exhibits a sharp, high-amplitude resonance peak at approximately 75 rad/s, reaching a relative amplitude of approximately 0.48. Beyond this resonance frequency, the parabolic profile system shows a secondary, smaller peak at approximately 310 rad/s before it diminishes at higher frequencies. The parabolic profile system oscillates when excited at its natural frequency. The linear profile system with α=0.2 and β=0.3 exhibited moderate resonance behaviour, with a primary relative amplitude of 0.23 occurring at approximately 85 rad/s. The relative amplitude developed was half that of the parabolic profile beam system. This indicates better damping characteristics than those of a parabolic profile beam system. Furthermore, the linear profile beam system exhibited a secondary peak at approximately 400 rad/sec, followed by a gradual decrease in amplitude. The uniform profile system (α=0.0 and β=0.0) displayed a controlled response among the three profile systems. Its primary resonance peak occurred at a similar frequency but had the lowest amplitude, approximately 0.13. Furthermore, the uniform profile system exhibited additional resonance modes at higher frequencies of approximately 450-500 Rad/Sec, suggesting a more complex dynamic behaviour. All three systems exhibited primary resonance in the low-frequency range of approximately 100 rad/s. However, their higher-order modal responses and damping properties differ significantly from each other.

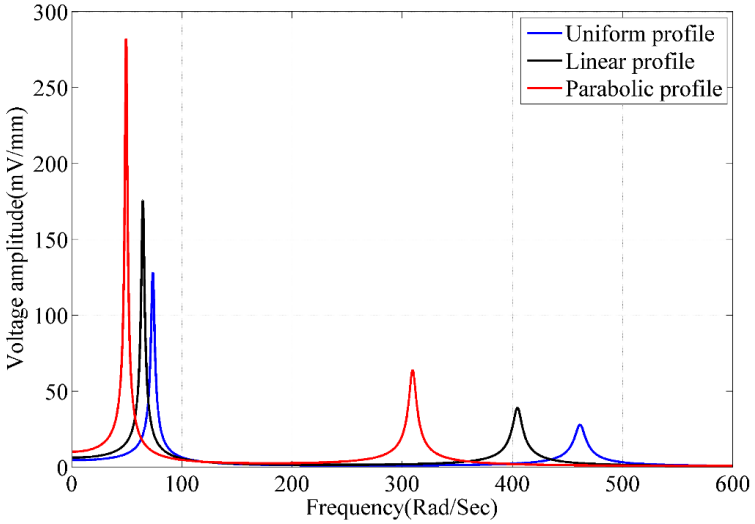


Figure 8. Voltage response of uniform beam (α = 0.0, β = 0.0), linear profile beam (α = 0.2, β = 0.3) and Parabolic profile beam (α = 0.2, β = 0.3)

Figure 8 shows the voltage response of the proposed beams with uniform, linear, and parabolic profile geometries, where the frequency range is from 0 to 600 rad/s. With α=0.2 and β=0.3, the parabolic profile exhibited the highest resonant response, reaching a voltage amplitude of approximately 280 mV/mm at 75 rad/s. Similarly, the linear profile exhibited a moderate resonance of 175 mV/mm at approximately 85 rad/s, and the uniform profile exhibited a maximum of 130 mV/mm at 80 rad/s. These sharp, narrow resonant peaks are due to highly selective frequency responses with less damping. These voltage-response characteristics are essential for designing and optimising beam-based transducers to select the appropriate profile geometries. Furthermore, the separation of the resonant frequencies also suggests the potential for multi-frequency operation using different profile sections. The upward shift in the voltage resonance frequency for parabolic profile beams can be attributed not only to the effect of the increased Young's modulus but also to the variation in the geometric stiffness toward the tip. This material gradation enhanced the stiffness, sharpened the resonant peak, and increased the voltage output.

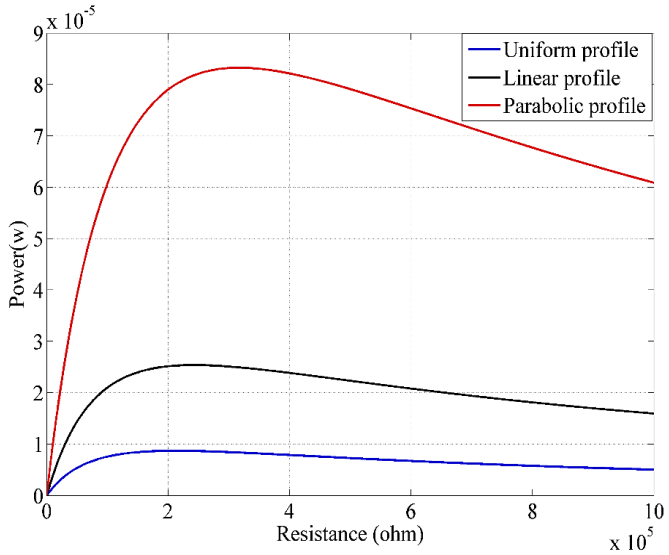


Figure 9. Power response of uniform beam (α = 0.0, β = 0.0), linear profile beam (α = 0.2, β = 0.3) and Parabolic profile beam (α = 0.2, β= 0.3)

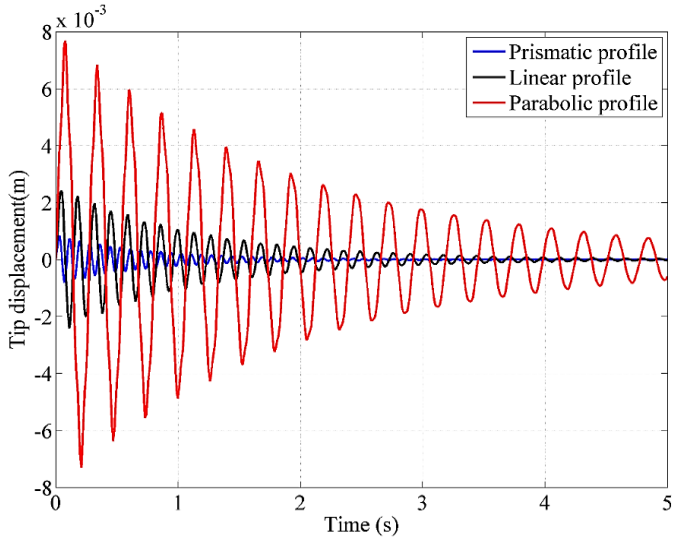


Figure 10. Tip displacement response of uniform beam (α = 0.0, β = 0.0), linear profile beam (α = 0.2, β = 0.3) and Parabolic profile beam (α = 0.2, β = 0.3) in time domain

The dynamic behaviour of three profile beam configurations subjected to time-varying excitation over five seconds is discussed. Figure 10 shows the tip displacement variation of the distinct profile beams subjected to a point load of 1 N at the free end of the beam structure. The parabolic profile beam exhibited large-amplitude oscillations that reached peak displacements of approximately 7.5×10^{-3} m in the positive direction and -6.5×10^{-3} m in the negative direction during the initial response phase. Subsequently, the response of the beam structure decayed exponentially, and the magnitude of the tip displacement amplitude gradually diminished. The linear-profile beam exhibited an intermediate dynamic characteristic, with maximum tip displacements of approximately 2.5×10^{-3} m during the initial stage of the response period. The frequency was higher than that of the parabolic profile beam, indicating that linear tapering provided increased structural stiffness for the dynamic response. Due to the linear geometry, the decay rate exhibits moderate damping characteristics. The tip displacement was approximately $\pm1\times10^{-3}$ m for a uniform-profile beam at the initial stage of the response period. Furthermore, the amplitude decayed rapidly, indicating a stiffer structural system. The extended oscillation period of the parabolic-profile beam indicates a higher energy storage capacity and lower structural damping, making it suitable for energy harvesting applications over an extended period. The gradual reduction in amplitude in all three cases reflects the natural energy dissipation through material and geometric effects. All three profile configurations showed an initial transient behaviour followed by a steady-state response, indicating stable system dynamics. The absence of amplitude growth indicates that the excitation frequency remains well-separated from the critical natural frequencies for each geometry.

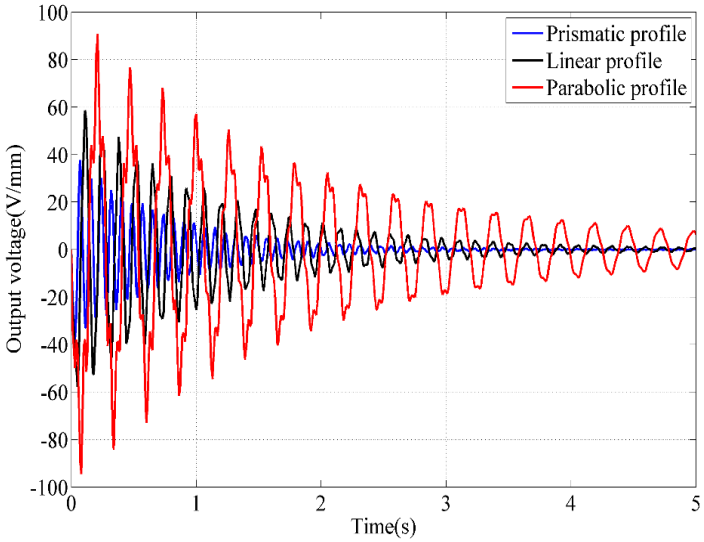


Figure 11. Voltage response of uniform beam (α = 0.0, β = 0.0), linear profile beam (α = 0.2, β = 0.3) and Parabolic profile beam (α = 0.2, β= 0.3) in time domain

Figure 11 shows the voltage-time response characteristics of an energy-harvesting system employing three distinct profile geometries over a period of five seconds. In the figure, the ordinate represents the normalised output voltage, whereas the abscissa represents the time period. From the figure, it is evident that the uniform-profile beam exhibits a constantly decaying oscillatory response, with initial voltage amplitudes of approximately 40 V/mm. The rapid decrease in the voltage amplitude indicates efficient energy dissipation through the harvesting mechanism. The linear profile beam indicated an initial voltage response of 30 V/mm, which subsequently decayed gradually. The parabolic-profile beam exhibited an initial voltage response of 80 V/mm, indicating the maximum energy extraction potential at the beginning of excitation. Subsequently, the response reached a steady state. The oscillation behaviour exhibits strong electromechanical coupling, which is used in applications that require instantaneous output power.

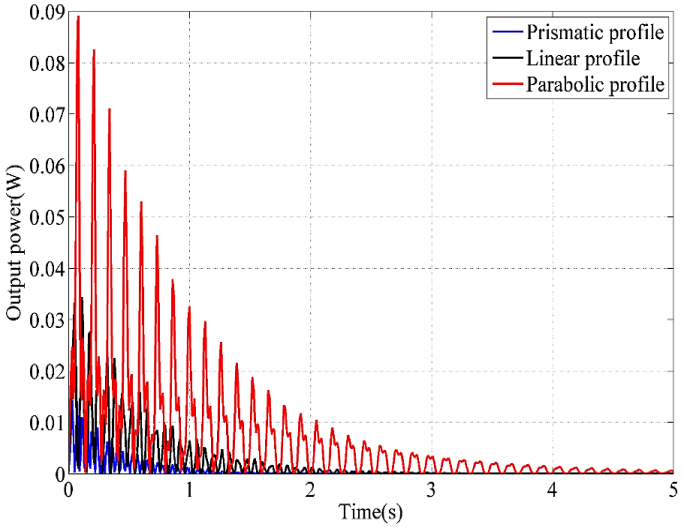


Figure 12. Output Power response of uniform beam (α = 0.0, β = 0.0), linear profile beam (α = 0.2, β = 0.3) and Parabolic profile beam (α = 0.2, β = 0.3) in time domain

Figure 12 shows the output power of the energy-harvesting system with the three different geometric profile configurations over five seconds. The output power (W) represents the ordinate, and the load resistance of the circuit represents the abscissa of the graph. In the initial period, the parabolic-profile beam reached a maximum power output of 0.09 W, which then decayed as time increased. This indicates the maximum power captured during the initial stage of oscillation, which is suitable for the instantaneous power. This is because of the strong electromechanical coupling between the beam structure and piezoelectric materials. The linear profile shows a power amplitude of 0.03 W, indicating controlled power oscillations compared to the parabolic profile structure. The uniform profile beam structure exhibited an output power of 0.015 W, which was lower than that of the parabolic and linear profile beam structures. The differences in performance observed among these three profiles, namely uniform, linear, and parabolic configurations, cannot be attributed to the geometry alone. Because all profile beams are axially functionally graded, the variations in mass density and stiffness affect the overall dynamic response of the beam structure. A uniform beam has a uniform bending stiffness-to-mass ratio along its length. Consequently, the beam developed a moderate resonance amplitude. By contrast, a

parabolic geometry profile improved this effect. The quadratic reduction in the cross-sectional area coincides with the linear increase in the modulus of elasticity, resulting in concentrated strain energy near the piezoelectric region near the fixed end. This increases the coupling between the material gradation and geometry, producing a higher output power. The uniform beam without taper variation exhibited lower electromechanical coupling and thus served as the benchmark for the other two beams.

4. Conclusions

This study presents a detailed numerical analysis of the energy-harvesting performance of axially functionally graded beam structures with varying geometric profiles. A finite element method developed in MATLAB was used to compare the natural frequencies, electrical voltage, harvested power, and overall energy conversion efficiency of piezoelectric-integrated beams. The axial functionally graded material properties along the length play a significant role in enhancing the electromechanical coupling. Three beam geometries, namely uniform, linearly tapered, and parabolically tapered, were analysed in this study. The analysis showed that the parabolic-profile beam exhibited higher fundamental frequencies and improved harvesting efficiency. The addition of proportional damping and a classic electrical interface improves the dynamic response. Both the tapering ratio and material gradation patterns strongly influence the maximum voltage and power output. The results provide practical design insights for high-efficiency energy harvesters for applications such as wireless sensor networks, structural health monitoring, and self-powered microelectromechanical system devices.

Acknowledgement

The authors gratefully acknowledge the support and encouragement received from DRIEMS University for their facilities and the guidance of their mentors throughout this research.

Funding

This study was not supported by any grants from funding bodies in the public, private, or non-profit sectors.

Declaration of Conflict of Interest

The authors declare no conflict of interest.

CRediT of Author Contributions

R.R. Senapati: Conceptualization, Methodology; Writing- review & revise
A. B. Dash : Analysis, Validation, Writing – Original Draft
S. Acharya : Methodology; Software, Formal Analysis
A. R. Biswal : Investigation; Data Curation, Methodology, Writing- review & revise
D. R. Biswal: Conceptualization; Methodology; validation; Supervision, Writing- review & revise

Availability of Data and Materials

The data supporting the findings of this study are available upon request from the corresponding author.

Ethics Declarations

This study did not involve human participants or animal subjects. Therefore, ethical approval was not required.

Generative Artificial Intelligence Declarations

The authors claim that artificial intelligence-assisted technologies, such as generative AI, were not used to generate content, ideas, or theories. We have used AI to enhance readability and refine the language. This was used with extreme human control and supervision. The authors take full responsibility for reviewing and approving the content.

References

[1] M. Rahmaty, "Energy harvesting technologies in a super-smart city," in *Energy-Efficient Transformative Technologies for Data-Driven Smart Cities*, pp. 55–70, 2026, https://doi.org/10.1016/b978-0-443-27618-7.00008-x.

[2] M. Iqbal, MM Nauman, FU Khan et al., "Vibration-based piezoelectric, electromagnetic, and hybrid energy harvesters for microsystems applications: A contributed review," *International Journal of Energy Research*, vol. 45, no. 1, pp. 65–102, 2021, https://doi.org/10.1002/er.5643.

[3] T. Sanislav, G. D. Mois, S. Zeadally, and S. C. Folea, "Energy harvesting techniques for Internet of Things (IoT)," *IEEE Access*, vol. 9, pp. 39530–39549, 2021. https://doi.org/10.1109/access.2021.3064066.

[4] A. Garg, W. Zheng, R. Raman, and L. Li, "Machine learning in functionally graded materials and nano FGMs: A comprehensive review of predictive modeling for mechanical behavior," *Archives of Computational Methods in Engineering*, vol. 33, no. 1, pp. 533–575, 2026, https://doi.org/10.1007/s11831-025-10316-6.

[5] V. Bhavar, P. Kattire, S. Thakare, and R. K. P. Singh, "A review on functionally gradient materials (FGMs) and their applications," in *IOP Conference Series: Materials Science and Engineering*, vol. 229, no. 1, p. 12021, 2017, https://doi.org/10.1088/1757-899x/229/1/012021.

[6] M. Kumar, M. Suhaib, N. Sharma, S. Kumar, and S. Choudhary, "Energy harvesting technologies in mechanical systems: A comprehensive review," *International Journal of Research Publication and Reviews*, vol. 5, pp. 2782–2787, 2024, https://doi.org/10.55248/gengpi.5.0124.0303.

[7] A. Singh, P. Kumari, and D. Sharma, "Axially functionally graded beams-a review," in *Asian Conference on Mechanics of Functional Materials and Structures*, pp. 479–496, 2022, https://doi.org/10.1007/978-981-99-5919-8_43.

[8] P. C. Ramegowda and D. Ishihara, "Accurate finite element modelling of multilayered flexible piezoelectric energy harvesting devices with strong coupling of structure, piezoelectricity, and circuit," *International Journal for Computational Methods in Engineering Science and Mechanics*, vol. 25, no. 3, pp. 137–151, 2024, https://doi.org/10.1080/15502287.2023.2291013.

[9] P. Hajheidari, I. Stiharu, and R. Bhat, "Performance of non-uniform functionally graded piezoelectric energy harvester beams," *Journal of Intelligent Material Systems and Structures*, vol. 31, no. 13, pp. 1604–1616, 2020, https://doi.org/10.1177/1045389x20930083.

[10] A. R. Biswal and D. R. Biswal, "Vibrational energy harvesting from functionally graded nonprismatic beams" *International Journal of Automotive and Mechanical Engineering*, vol. 22, no. 2, pp. 12359–12372, 2025, https://doi.org/10.15282 /ijame.22.2.2025.9.0946

[11] S. Pal and D. Das, "Free vibration response of bidirectional functionally graded rotating micro-disk under mechanical and thermal loading," *The Journal of Strain Analysis for Engineering Design*, vol. 58, no. 7, pp. 517–537, 2023, https://doi.org/10.1177/03093247231160617.

[12] T. Yu, F. Liang, and H. Yang, "Vibration energy harvesting of a three-directional functionally graded pipe conveying fluids," *Applied Mathematics and Mechanics*, vol. 46, no. 5, pp. 795–812, 2025, https://doi.org/10.1007/s10483-025-3249-8.

[13] B. Gupta, P. Sharma, and S. K. Rathore, "A new numerical modelling of an axially functionally graded piezoelectric beam," *Journal of Vibration Engineering & Technologies*, vol. 10, no. 8, pp. 3191–3206, 2022, https://doi.org/10.1007/s42417-022-00550-8.

[14] K. Bendine, J. L. J. Pereira, and G. F. Gomes, "Energy harvesting enhancement of nonuniform functionally graded piezoelectric beam using artificial neural networks and Lichtenberg algorithm," in *Structures*, vol. 57, p. 105271, 2023, https://doi.org/10.1016/j.istruc.2023.105271.

[15] P. Zhang, Z. Peng, H. Xu, and J. Peng, "Modal Characteristics of axially functionally graded beams carrying additional masses," *Mechanics of Solids*, pp. 1–20, 2025, https://doi.org/10.1134/s0025654425600904.

[16] A. A. Daikh et al., "Static analysis of functionally graded plate structures resting on variable elastic foundation under various boundary conditions," *Acta Mechanica*, vol. 234, no. 2, pp. 775–806, 2023, https://doi.org/10.1007/s00707-022-03405-1.

[17] N.D. Nguyen, "A new higher-order beam theory for buckling and free vibration responses of laminated composite and functionally graded porous beams," *The Journal of Strain Analysis for Engineering Design*, vol. 59, no. 1, pp. 67–81, 2024, https://doi.org/10.1177/03093247231187454.

[18] M. Heshmati, F. Daneshmand, and Y. Amini, "Vibration and stability analysis of functionally graded elliptical pipes conveying fluid with flow velocity profile modification," *Engineering with Computers*, pp. 1–16, 2023, https://doi.org/10.1007/s00366-021-01541-1.

[19] B. Wang, X. Luo, Y. Liu, and Z. Yang, "Thickness-variable composite beams for vibration energy harvesting," *Composite Structures*, vol. 244, p. 112232, 2020, https://doi.org/10.1016/j.compstruct.2020.112232.

[20] M. Mousavi, S. Ziaei-Rad, and A. H. Karimi, "Piezoelectric-based energy harvesting from bridge vibrations subjected to moving successive vehicles by functionally graded cantilever beams –Theoretical and experimental investigations," *Mechanical Systems and Signal Processing*, vol. 188, p. 110015, 2023, https://doi.org/10.1016/j.ymssp.2022.110015.

[21] R. Singh and P. Sharma, "Vibration analysis of an axially functionally graded material non-prismatic beam under axial thermal variation in a humid environment," *Journal of Vibration and Control*, vol. 28, no. 23–24, pp. 3608–3621, 2022, https://doi.org/10.1177/10775463211037150.

[22] M. H. Mansor, M. S. M. Sani, M. F. Hassan, and L. Tang, "Fully-coupled modelling and experimental validation of quarter wavelength resonator with piezoelectric backplate in vibro-acoustic energy harvesting," *International Journal of Automotive and Mechanical Engineering*, vol. 22, no. 2, pp. 12511–12527, 2025, https://doi.org/10.15282/ijame.22.2.2025.19.0956

[23] J. Zhang, Y. Wang, X. Liu, "Significantly enhanced energy harvesting performance in piezoelectric energy harvesters through synergistic structural design," *Materials Horizons*, vol. 12, no. 10, pp. 3494-3504, 2025, https://doi.org/10.1039/d4mh01902d.

[24] S. Dao, Nguyen, D. Nguyen, N. Nguyen, D.Thai, "A closed-form solution for harvesting energy from the vibrations of sandwich beams under impact loading," *Buildings*, vol. 15, no. 12, p. 2135, 2025, https://doi.org/10.3390/buildings15122135.

[25] M. H. Abdelati, A. H. Matar, M. Mourad, and M. Rabie, "Evaluating sensor placement in vibration-based engine misfire detection using artificial neural networks," *International Journal of Automotive and Mechanical Engineering*, vol. 22, no. 3, pp. 12603–12613, 2025. https://doi.org/10.15282/ijame.22.3.2025.5.0962.

[26] MK. Khorramabadi Free vibration of functionally graded beams with piezoelectric layers subjected to axial load. *Journal of Solid Mechanics*, vol. 1, no. 1, pp. 22-28, 2009, https://doi.org/10.1007/s10483-009-0803-7.

[27] A. Benjeddou, S.R. Mahmoud, M.A. Eltaher, "Active vibration control of functionally graded beams with piezoelectric layers based on higher-order shear deformation theory," *Composite Structures*, vol. 152, pp. 391–404, 2016, https://doi.org/10.1007/s11803-016-0352-y.

[28] Z. G. Ruan, Z.-G. Ying, H. Lei, L. Xia, and W. Wang, "Base-excited random vibration of quasi-periodic controllable viscoelastic sandwich plates with distributed supporting masses," Mechanics of Advanced Materials and Structures, vol. 33, no. 1, p. 2681941, 2026, https://doi.org/10.1080/15376494.2026.2681941.

[29] A. Abdelkefi "Aeroelastic energy harvesting: A review," *International Journal of Engineering Science*, vol. 100, pp. 112–135, 2016, https://doi.org/10.1016/j.ijengsci.2015.10.006.

[30] F. Tornabene, N. Fantuzzi, M. Bacciocchi, "Free vibration analysis of functionally graded structures using advanced finite element formulations," *Composite Structures*, vol. 132, pp. 385–410, 2015.

[31] A. Erturk, D. J. Inman, *Piezoelectric Energy Harvesting*. Chichester: John Wiley & Sons; 2011, https://doi.org/10.1002/9781119991151.

[32] L. Guo and Y. Qin, "Modelling and analysis of a bimorph piezoelectric cantilever," in *2016 13th International Conference on Ubiquitous Robots and Ambient Intelligence* (URAI), pp. 248–251, 2016, https://doi.org/10.1109/urai.2016.7625748.

[33] A. Khan, M. Q. Nawaz, and L. Xu, "Investigation and numerical simulation of different piezoelectric bimorph cantilever designs for energy harvesting," *International Journal of Electrical, Energy and Power System Engineering*, vol. 7, no. 2, pp. 85–99, 2024, https://doi.org/10.31258/ijeepse.7.2.85-99.

[34] A. Erturk and D. J. Inman, "An experimentally validated bimorph cantilever model for piezoelectric energy harvesting from base excitations," *Smart Materials and Structures*, vol. 18, p. 025009, 2009, https://doi.org/10.1088/0964-1726/18/2/025009.

[35] M. A. Elgamal, H. Elgamal, and S. A. Kouritem, "Optimised multi-frequency nonlinear broadband piezoelectric energy harvester designs," *Scientific Reports*, vol. 14, no. 1, p. 11401, 2024. https://doi.org/10.1038/s41598-024-61355-1.